A novel internal heat recycling concept for reducing energy consumption and increasing flux through three-stage air-gap–water-gap membrane distillation system

Mostafa Abd El-Rady Abu-Zeid, Xiaolong Lu and Shaozhe Zhang

ABSTRACT

The low flux and high energy consumption problems of the conventional three-stage air-gap membrane distillation (AG-AG-AG)MD system caused by the low temperature difference between hot and cold feed at both sides of the membrane and high boundary layer thickness were solved successfully by replacing one of the three stages of air gaps by a water gap. The novel three-stage air-gap–water-gap membrane distillation (AG-AG-WG)MD system reduced energy consumption and increased flux due to efficient internal heat recycling by virtue of a water-gap module. Heat and mass transfer in novel and conventional three-stage systems were analyzed theoretically. Under a feed temperature of 45 °C, flow rate of 20 l/h, cooling temperature of 20 °C, and concentration of 340 ppm, the (AG-AG-WG)MD promoted flux by 17.59% and 211.69%, and gained output ratio (GOR) by 60.57% and 204.33% compared with two-stage (AG-WG)MD and one-stage AGMD, respectively. This work demonstrated the important role of a water gap in changing the heat and mass transfer where convection heat transfer across the water gap is faster by 24.17 times than conduction heat transfer through the air gap. The increase in flux and GOR economized the heating energy and decreased waste heat input into the system. Additionally, the number of MD stages could increase the achieving of a high flux with operation stability.

Key words | combined air-gap-water-gap MD, heat and mass transfer, internal heat recycling, multi-stage AGMD, water-gap module

Mostafa Abd El-Rady Abu-Zeid (corresponding author)
Xiaolong Lu
Shaozhe Zhang
Institute of Biological and Chemical Engineering, State Key Laboratory of Separation Membranes and Membrane Processes, School of Material Science and Engineering,
Tiangong University,
Tianjin, 300387,
China
E-mail: *mostafa241981@agr.suez.edu.eg*

Mostafa Abd El-Rady Abu-Zeid
Department of Agricultural Engineering, Faculty of Agriculture,
Suez Canal University,
Ismailia 41522,
Egypt

HIGHLIGHTS

- A combined air-gap and water-gap MD system succeeded in reducing the energy consumption and promoted the vapor flux efficiently.
- The heat and mass transfer process in both of the AGMD and WGMD systems are presented here.
- The module of a water-gap MD has improved largely the multi-stage AGMD system performance.

NOMENCLATURE

AGMD	Air-gap membrane distillation
WGMD	Water-gap membrane distillation
(AG-WG)MD	Air-gap–water-gap membrane distillation
$C_{\text{saline water}}$	Salt concentration of feed saline water (%)
$C_{\text{permeate water}}$	Salt concentration of permeate water (%)
C_{pf}	Specific heat capacity of hot feed solution (J/kg·°C)
$C_{\text{pmem.}}$	Specific heat capacity of membrane material (J/kg·°C)
$C_{\text{mem.}}$	A constant referring to a mass transfer mechanism style inside the membrane (J/kg·°C)

doi: 10.2166/ws.2020.184

$C_{\text{air gap}}$	Molecular diffusion coefficient within the air gap (J/kg·°C)
C_{Pw}	Specific heat of water (J/kg·°C)
ESA	Effective evaporation surface area in accordance with internal diameter of the PVDF hollow fiber membrane (m^2)
$Q_{\text{hot feed, conv.}}$	The heat transported from the hot feed bulk solution to the membrane surface by convection (kJ/h)
$Q_{\text{hot feed, diffus.}}$	The heat transported from the hot feed bulk solution to the membrane surface by diffusion (kJ/h)
$Q_{\text{mem., condu.}}$	The heat transported through the membrane matrix via conduction (kJ/h)
$Q_{\text{mem, latent heat}}$	The heat transported through the membrane matrix via evaporation latent heat (kJ/h)
$Q_{\text{mem, sensible heat}}$	The heat transported through the membrane matrix via sensible heat (kJ/h)
$Q_{\text{film, condu.}}$	The heat transported through the condensate film thickness via conduction (kJ/h)
$Q_{\text{film, conv.}}$	The heat transported through the condensate film thickness via convection (kJ/h)
$Q_{\text{surface, condu.}}$	The heat transported by conduction through condensing surface thickness (kJ/h)
$Q_{\text{cold feed, conv.}}$	Convective heat transfer in the bulk cold fluid (kJ/h)
$Q_{\text{l.h., permeate water}}$	Latent heat of vapor flux (kJ/h)
$Q_{\text{h.i}}$	Specific waste heat input (MJ/kg)
$h_{\text{hot feed}}$	Convective heat transfer coefficient through the hot feed (W/(m^2·°C))
$h_{\text{mem.}}$	Heat transfer coefficient through the membrane (W/(m^2·°C))
$h_{\text{water gap}}$	Heat transfer coefficient within the water-gap (W/(m^2·°C))
h_{film}	Heat transfer coefficient through the condensate film (W/(m^2·°C))
$h_{\text{cold feed}}$	Convective heat transfer coefficient through the cold feed (W/(m^2·°C))
GOR	Gained output ratio (dimensionless)
$K_{\text{mem.}}$	Membrane thermal conductivity (W/(m·°C))
$K_{\text{air gap}}$	Air thermal conductivity (W/(m·°C))
K_{film}	Thermal conductivity of condensate film (W/(m·°C))
K_{surface}	Thermal conductivity of condensing surface (W/(m·°C))
M_{f}	Feed flow rate (l/h)
M_{m}	Water molar mass (≈18 g/mol)
$P_{\text{v,feed}}$	Partial vapor pressure at feed side (MPa)
$P_{\text{v,air gap}}$	Partial vapor pressure at air-gap side (MPa)
SRF	Salt rejection factor (%)
STEC	Specific thermal energy consumption (kWh/kg)
t	Time (minute)
T_{f}	Hot bulk feed temperature (°C)
T_{fm}	Hot feed temperature at the membrane surface (°C)
$T_{\text{fm,1}}$	Temperature of the membrane surface from the air-gap side (°C)
T_{pr}	Temperature of the condensate film from the air-gap side (°C)
$T_{\text{c,1}}$	Temperature of the condensate film near to condensing surface (°C)
$T_{\text{c,2}}$	Temperature of the condensing surface from the cold feed side (°C)
T_{c}	Cold feed bulk temperature (°C)
ΔT_{cross}	Temperature difference between the evaporator inlet ($T_{\text{evap.,inlet}}$) and the condenser outlet ($T_{\text{cond.,outlet}}$) (°C)
ΔH_{V}	Evaporative latent heat (≈2,326 kJ/kg)
F_{wv}	Water vapor flux (kg/(m^2·h))
$F_{\text{WV, air gap}}$	Mass vapor transported by diffusion style within the air gap (kg/(m^2·h))
$F_{\text{WV, water gap}}$	Mass vapor transported by diffusion style within the water gap (kg/(m^2·h))
$\delta_{\text{mem.}}$	Membrane thickness (m)
$\delta_{\text{air gap}}$	Thickness of air gap (m)
δ_{film}	Thickness of condensate film (m)
δ_{surface}	Thickness of condensing surface (m)
φ	Ideal gas constant (≈8.3145 J/mol·K)
W_{wv}	Weight of distilled water (kg)
$h_{\text{universal}}$	Universal membrane coefficient (kg/(m^2·h)·mbar)

h_d Diffusive coefficient through membrane (kg/(m^2 h)·mbar)

h_c Free convective coefficient through air gap (kg/(m^2·h)·mbar)

INTRODUCTION

Membrane distillation (MD) is a thermally driven separation process that has emerged as a motivating alternative to the current prevalent desalination systems like reverse osmosis (RO) and multi-stage flash (MSF). Some researchers (*e.g.* Hickenbottom & Cath 2014; Lee *et al.* 2016) used MD as a supplementary process attached squarely to the RO and MSF plants due to the lesser footprint demand, low sensitivity to heavy salt concentrations, and potential working at small-scale applications. The quantity of pure distilled water obtained from seawater or brackish water using MD primarily relies upon the available temperature difference between the warm fluid and the cold fluid which affects profoundly the generated vapor pressure difference (i.e., permeation driving force). The produced vapor molecules are transmitted from the interfaces of liquid/vapor at the feed side and then dry membrane pores to be condensed and converted at the end into pure distilled water on the exterior cooling surface at the membrane permeate side (Martínez & Rodríguez-Maroto 2008; Zhao *et al.* 2013; Lu *et al.* 2017). Air-gap membrane distillation (AGMD) and water-gap membrane distillation (WGMD) are two of the most common MD processes as well as material gap (MGMD), direct contact (DCMD), and vacuum membrane distillation (VMD) (Zhang *et al.* 2009; Francis *et al.* 2013; Khalifa *et al.* 2014; Khalifa 2015; Sivakumar *et al.* 2015; Ebadi *et al.* 2019; Shahu & Thombre 2020). AGMD and WGMD processes are distinguished by the capability of yielding distilled water with zero salts (Cath *et al.* 2004; El-Bourawi *et al.* 2006; Khayet & Matsuura 2011) using high intensity salt concentration solution (Khayet & Matsuura 2011; Xu *et al.* 2016) under low operating pressure (Laganà *et al.* 2000; Alkhudhiri *et al.* 2012) and temperature (El-Bourawi *et al.* 2006; Alkhudhiri *et al.* 2012). Further, the AGMD process has two more interesting characteristics that have given it advanced standing for salt fluid desalination through pilot investigation systems (Schwantes *et al.* 2013; Alsaadi *et al.* 2015). Firstly, latent heat of condensation could be completely recovered inside the membrane module without wanting a heat exchanger/vacuum pump as in sweeping gas (SGMD)/vacuum membrane distillation (VMD) (Guijt *et al.* 2005; Koschikowski *et al.* 2009; Khayet & Matsuura 2011; Alsaadi *et al.* 2013, 2015; Duong *et al.* 2015; Xu *et al.* 2016). Secondly, the thermal insulation area constituted by the air gap between the membrane and the cooling plate minimized deeply the heat loss by conduction through the membrane matrix, leading to appreciable improvement in AGMD thermal efficiency in comparison with DCMD. But some investigators (e.g. Minier-Matar *et al.* 2014; Wang & Chung 2015) mentioned this area imposes additional mass transfer impedance, leading to flux impoverishment as well as feed side thermal-concentration boundary layers, low membrane operation stability, membrane fouling, and wetting, finally reducing the chance of investment extensively (Alkhudhiri *et al.* 2012; Cipollina *et al.* 2012; Hawlader *et al.* 2012; Saffarini *et al.* 2012; Alsaadi *et al.* 2013; Minier-Matar *et al.* 2014; Khalifa *et al.* 2015).

The multi-stage system accompanied by internal heat recovery has been endorsed as an achievable technique to enrich the vapor flux and decrease the thermal energy consumption which has already been applied successfully in several experimental investigations (*e.g.* Hogan *et al.* 1991; Ding *et al.* 2005; Guillén-Burrieza *et al.* 2011; Zhao *et al.* 2013; Lee & Kim 2014; Shim *et al.* 2014; González-Bravo *et al.* 2015; Kim *et al.* 2015; Abu-Zeid & ElMasry 2020). Furthermore, Khalifa *et al.* (2017) reported that the water flux system of a multi-stage AGMD connected in series and parallel was maximal about 2.6–3.0 times more than the water flux system composing of only one stage. Likewise, the vapor flux module of a multi-stage AGMD was greater compared with the vapor flux produced from a one-stage system (Geng *et al.* 2015). Yao *et al.* (2012) proclaimed thermal efficiency of 80% and a performance ratio of 13.8 by virtue of a continuous-effect AGMD module designed with internal heat recovery. Pangarkar & Deshmukh (2015) improved profoundly the permeation flux of the AGMD system composed of four stages prepared specifically for a water treatment process, reaching up to 166.4 kg/(m^2·h). In another work, a zero-liquid discharge was fulfilled through a successful combination between a multi-stage flat sheet AGMD module and an evaporative crystallizer (Guo *et al.* 2016).

Lawal & Khalifa (2015) stated that the performance of an AGMD system composed of two stages (128.46 kg/(m^2·h) flux) was better compared with a one-stage AGMD system (65.81 kg/(m^2·h) flux) at different operating conditions. Later, Lee *et al.* (2019) reported an exciting value for gained output ratio (GOR) reaching up to 24.4 through a fruitful connection between a multi-stage AGMD reversal design and a system of natural/forced cooling corresponding to only 3.89 without a natural cooling system.

However, despite the important role of the multi-stage system in vapor flux enrichment and energy consumption reduction, the quantity of pure distilled water obtained from each stage is inversely proportional to the number of incorporated stages because of the significant temperature drop and feed salinity increase which affects profoundly the temperature difference across the membrane, heat and mass transport; especially when a highly saline water is used as feed. Thence, the present research work focused on achieving the following aims:

1. Upgrade the system performance of three-stage air-gap membrane distillation (AGMD) by incorporation of it with the water-gap module consecutively.
2. Carry out a comparative study between the systems of three-stage and two-stage air-gap–water-gap membrane distillation (AG-WG)MD with the system of one-stage AGMD respecting vapor flux (F_{wv}) and gained output ratio (GOR).
3. Analysis of heat and mass transfer mechanism theoretically for the systems of the three-stage (AG-WG)MD and AGMD.

The key idea of inserting the water-gap module into the system of the three-stage AGMD is to take advantage of water-gap characteristics (*e.g.* efficient internal heat recovery, low impedance to mass transfer, and less heat loss through the permeate water) in decreasing the thermal-concentration feed side boundary layer thickness, increasing the trans-membrane temperature difference, and stimulating the heat and mass transport through the integrated AGMD stages.

To implement this idea in a laboratory, a system of three-stage AGMD composed of three similar air-gap MD modules was installed and tested experimentally. After that, the obtained results from the system of three-stage AGMD were compared with the results of one-stage AGMD, two–stage (AG-WG)MD, and three-stage (AG-WG)MD systems. The last two systems are composing of one water-gap module fixed mutually at different positions before, between, and after the air-gap modules. A set of equations were used to analysis in theory the heat and mass transport through various three-stage MD systems with and without the water-gap module. The experimental investigations were performed at different feed temperatures, feed flow rates, and feed salt concentrations. The performances of different three-stage, two-stage, and one-stage systems were evaluated respecting vapor flux (F_{wv}), gained output ratio (GOR), thermal energy consumption (STEC), and waste heat input ($Q_{h.i}$). The membrane modules of the air gap and water gap were designed with internal heat recovery.

THE MECHANISM OF HEAT AND MASS TRANSFER IN THE SYSTEMS OF THREE-STAGE AGMD AND (AG-WG)MD

The heat and mass transfer process within the membrane distillation (MD) module are executed concurrently with a continual flowing of warm and cold fluids in a counter-current direction at the hot feed and the cold permeate sides. As elaborated schematically in Figures 1 and 2, the heat and mass transfer within the presently studied air-gap and water-gap membrane modules are done via convection, conduction, and evaporation.

Heat transfer within AGMD module

Heat transfer through the hot feed side from feed bulk to membrane surface is carried out via convection ($Q_{\text{hot feed, conv.}}$) and diffusion ($Q_{\text{hot feed, diffus.}}$) (Sharqawy *et al.* 2010; Khalifa *et al.* 2015):

$$Q_{\text{hot feed, conv.}} = h_{\text{hot feed}} \times (T_f - T_{fm}) \quad (1)$$

$$Q_{\text{hot feed, diffus.}} = (F_{wv} - C_{Pf}) \times (T_f - T_{fm}) \quad (2)$$

where T_f and T_{fm} are the hot feed temperature at bulk and membrane surface (°C), $h_{\text{hot feed}}$ is the convective heat transfer coefficient through the hot feed (W/(m^2·°C)), F_{wv} is the water vapor flux (kg/(m^2.h)), and C_{Pf} is the specific heat capacity of the hot feed (J/kg·°C).

Heat transfer across the membrane by conduction ($Q_{\text{mem., condu.}}$), evaporation latent heat ($Q_{\text{mem., latent heat}}$),

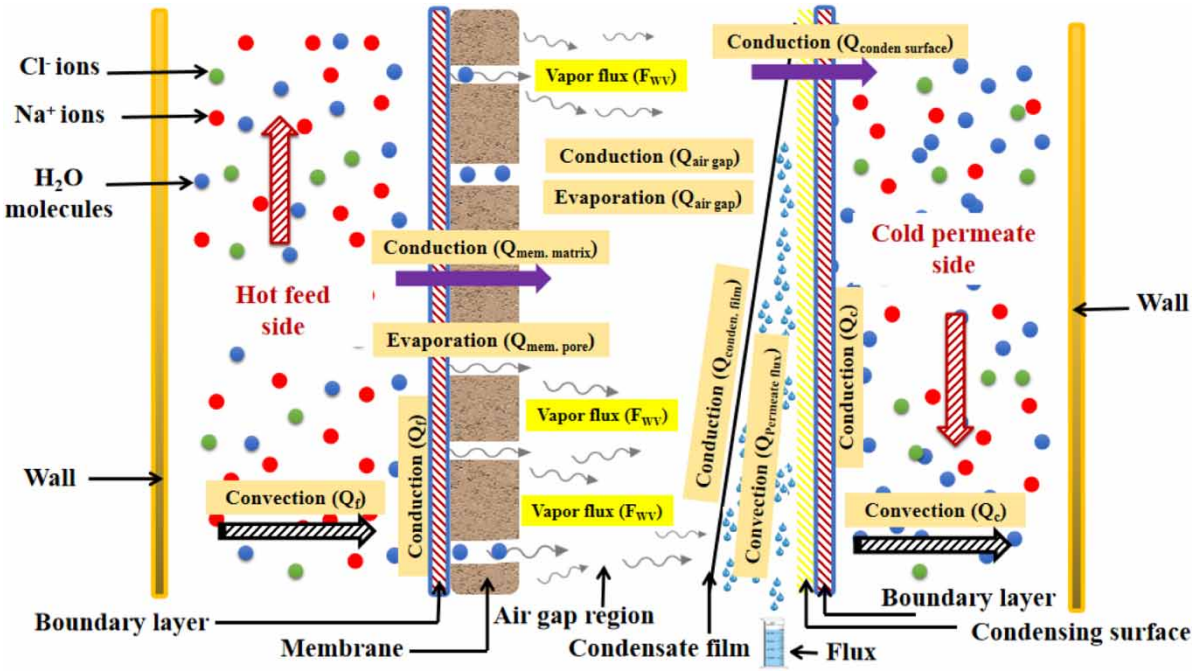

Figure 1 | The heat and mass transfer within the AGMD module.

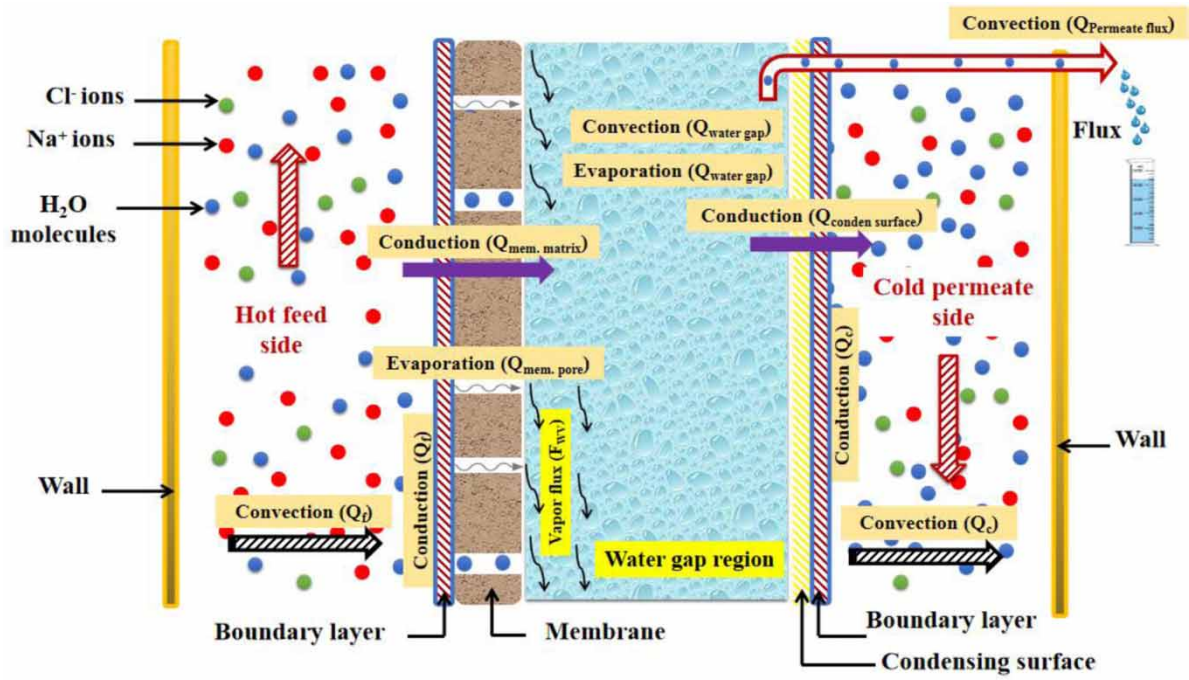

Figure 2 | The heat and mass transfer within the WGMD module.

and sensible heat ($Q_{\text{mem., sensible heat}}$) can be given as follows (Geng *et al.* 2014; Khalifa *et al.* 2015):

$$Q_{\text{mem., condu.}} = \frac{K_{\text{mem.}}}{\delta_{\text{mem.}}} \times (T_{\text{fm}} - T_{\text{fm,1}})$$

$$Q_{\text{mem., condu.}} = h_{\text{mem.}} \times (T_{\text{fm}} - T_{\text{fm,1}}) \quad (3)$$

$$Q_{\text{mem., latent heat}} = F_{\text{wv}} \times \Delta H_{\text{V}} \quad (4)$$

$$Q_{\text{mem., sensible heat}} = F_{\text{wv}} \times C_{\text{p mem.}} \times (T_{\text{fm}} - T_{\text{fm,1}}) \quad (5)$$

where $K_{\text{mem.}}$ is the membrane thermal conductivity (W/(m·°C)), $\delta_{\text{mem.}}$ is the membrane thickness (m), $T_{\text{fm,1}}$ is the temperature of the membrane surface at the air-gap side (°C), $h_{\text{mem.}}$ is the heat transfer coefficient through the membrane (W/(m^2·°C)), and $C_{\text{p mem.}}$ is the specific heat capacity of the membrane material (J/kg·°C), and ΔH_{V} is the evaporative latent heat (≈2,326 kJ/kg).

The heat transfer within the air-gap area is done by conductive and evaporative latent heat, meanwhile when the gap area is filled wholly with the condensed water vapor the heat is transferred by convection instead of conduction:

$$Q_{\text{air gap, condu.}} = \frac{K_{\text{air gap}}}{\delta_{\text{air gap}}} \times (T_{\text{fm,1}} - T_{\text{pr}}) \quad (6)$$

$$Q_{\text{air gap, latent heat}} = F_{\text{wv}} \times \Delta H_{\text{V}} \quad (7)$$

$$Q_{\text{water gap, convec.}} = h_{\text{water gap}} \times (T_{\text{fm,1}} - T_{\text{pr}}) \quad (8)$$

where $K_{\text{air gap}}$ is the air thermal conductivity (W/(m·°C)), $\delta_{\text{air gap}}$ is the thickness of the air gap (m), T_{pr} is the temperature of the condensate film from the air-gap side (°C), and $h_{\text{water gap}}$ is the heat transfer coefficient within the water-gap area (W/(m^2·°C)).

Heat transfer across the condensate film thickness is performed by means of conduction ($Q_{\text{film, condu.}}$) and convection ($Q_{\text{film, conv.}}$), which can be calculated as:

$$Q_{\text{film., condu.}} = \frac{K_{\text{film}}}{\delta_{\text{film}}} \times (T_{\text{pr}} - T_{\text{c,1}}) \quad (9)$$

$$Q_{\text{film., conv.}} = h_{\text{film}} \times (T_{\text{pr}} - T_{\text{c,1}}) \quad (10)$$

where K_{film} is the thermal conductivity of the condensate film (W/(m·°C)), δ_{film} is the thickness of the condensate film (m), h_{film} is the heat transfer coefficient through the condensate film thickness (W/(m^2·°C)), and $T_{\text{c,1}}$ is the temperature of the condensate film near to the condensing surface (°C).

The conductive heat transfer through the condensing surface can be determined mathematically by using the following equation:

$$Q_{\text{surface, condu.}} = \frac{K_{\text{surface}}}{\delta_{\text{surface}}} \times (T_{\text{c,1}} - T_{\text{c,2}}) \quad (11)$$

where K_{surface} is the thermal conductivity of the condensing surface (W/(m·°C)), δ_{surface} is the thickness of the condensing surface (m), and $T_{\text{c,2}}$ is the temperature of the condensing surface from the cold feed side (°C).

The convective heat transfer through the cold bulk at the permeate side is given by:

$$Q_{\text{cold feed., conv.}} = h_{\text{cold feed}} \times (T_{\text{c,2}} - T_{\text{c}}) \quad (12)$$

where T_{c} is the cold feed bulk temperature (°C) and $h_{\text{cold feed}}$ is the convective heat transfer coefficient through the cold feed (W/(m^2·°C)).

Heat transfer within WGMD module

The heat transfer across the water-gap module is similar to the heat transfer across the air-gap module excepting the heat transfer within the air-gap area which is replaced by heat transfer via evaporation and convection through the permeate water.

Mass transfer within AGMD module

The mass transfer through the membrane is qualified by both Knudsen and molecular diffusion, and through the air-gap area symbolized by ($F_{\text{WV,air gap}}$) it is done via free convection. The quantity of $F_{\text{WV,air gap}}$ can be estimated using the following equations (Cussler 1997; Bouguecha *et al.* 2002; Khayet & Matsuura 2011; Cipollina *et al.* 2012; Alsaadi *et al.* 2013):

$$F_{\text{WV,air gap}} = h_{\text{universal}} \times \Delta P_{\text{v (feed – air gap)}} \quad (13)$$

$$F_{\text{WV,air gap}} = M_m \times \frac{h_{\text{universal}}}{\varphi} \times (P_{\text{v,feed}} - P_{\text{v,air gap}}) \quad (14)$$

where M_{m} is the water molar mass (≈18 g/mol), φ is the ideal gas constant (≈8.3145 J/mol·K), $P_{\text{v,feed}}$ and $P_{\text{v,air gap}}$ are the partial vapor pressure at feed and air-gap sides

(MPa), and $h_{universal}$ is the universal membrane coefficient (kg/(m^2.h).mbar), which can be described as:

$$h_{universal} = \left(\frac{1}{h_d^{-1} + h_c^{-1}}\right) \quad (15)$$

where h_d is the diffusive coefficient across the membrane (kg/(m^2.h).mbar), and h_c is the free convective coefficient through the air gap (kg/(m^2·h).mbar). The values of $h_{universal}$ are placed in the range either between 3×10^{-10} m^3/m^{2}s·Pa and 7×10^{-10} m^3/m^{2}s·Pa or between 0.10 kg/(m^2·h).mbar and 0.25 kg/(m^2·h)·mbar (García-Payo *et al.* 2000).

Mass transfer within WGMD module

In view of no/weak impedance to mass transfer during the WGMD process, the vapor quantity transferred across the membrane of the water gap ($F_{WV,water\ gap}$) is much higher than that in the air gap ($F_{WV,air\ gap}$). Additionally, the heat transfer by convection across the water gap is faster by 24.17 times than the heat transfer by conduction through the air gap (i.e., the thermal conductivity of water is 0.58 W/m·K and the thermal conductivity of air is 0.024 W/m·K). This behaviour can be viewed obviously in Figure 3, which illustrates the formation of thermal-concentration feed side boundary layers during the system of three-stage AGMD with a low temperature difference across the membrane, which profoundly influences the heat and mass transport and the vapor flux correspondingly. In contrast, Figure 4 elucidates no thermal-concentration boundary layers at the feed side during the system of three-stage air-gap–water-gap (AG-WG)MD with a high temperature difference across the membrane due to the function of the water-gap module in making a tangible change in the heat and mass transport and enriching the flux.

MATERIALS AND METHODS

Three-stage AGMD and (AG-WG)MD set-up

Sketches of the three-stage AGMD and (AG-WG)MD systems installed in a vertical direction are elucidated in Figure 5(a)–5(d). The three-stage AGMD symbolized as (AG-AG-AG)MD is used as a reference system for comparison with different systems of three-stage (AG-WG)MD symbolized as (WG-AG-AG)MD, (AG-WG-AG)MD, and (AG-AG-WG)MD. The sketches of the two-stage (AG-WG)MD and one-stage AGMD systems are not included here as they are similar to current systems excepting only the number of incorporated stages. The systems consist of feeding tank, membrane modules, circulation pump MP-55RZ (Shanghai Xinxishan Industrial Limited Company, China), rotameter LZB-4 (Huanming, Yugao Industrial Automation Instrument Company, Zhejiang, China), valves, thermostatic water bath CS-501 (Tongzhou Branch of Shanghai Jinping

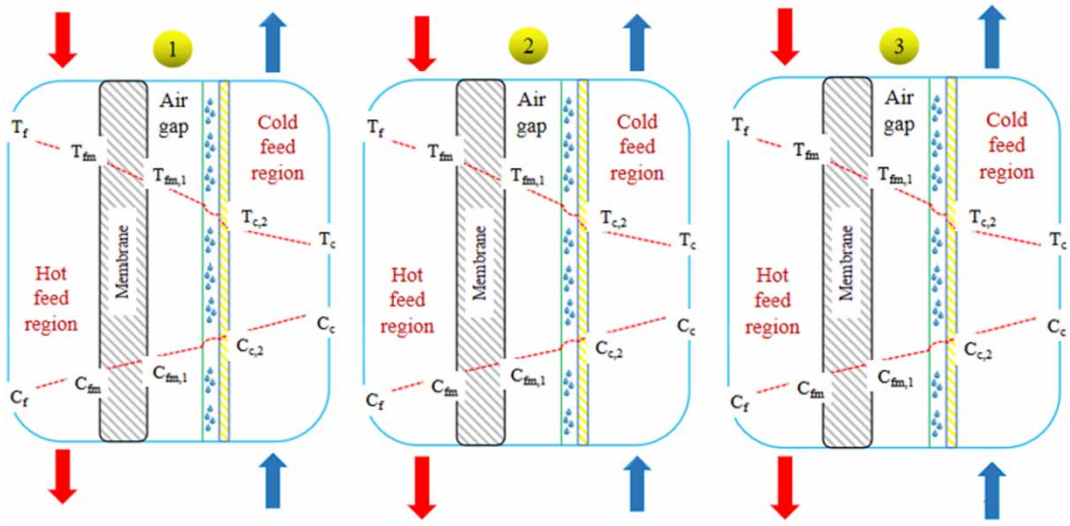

Figure 3 | The sketch shows thermal-concentration boundary layers formed at the feed side of the three-stage AGMD system with low trans-membrane temperature difference.

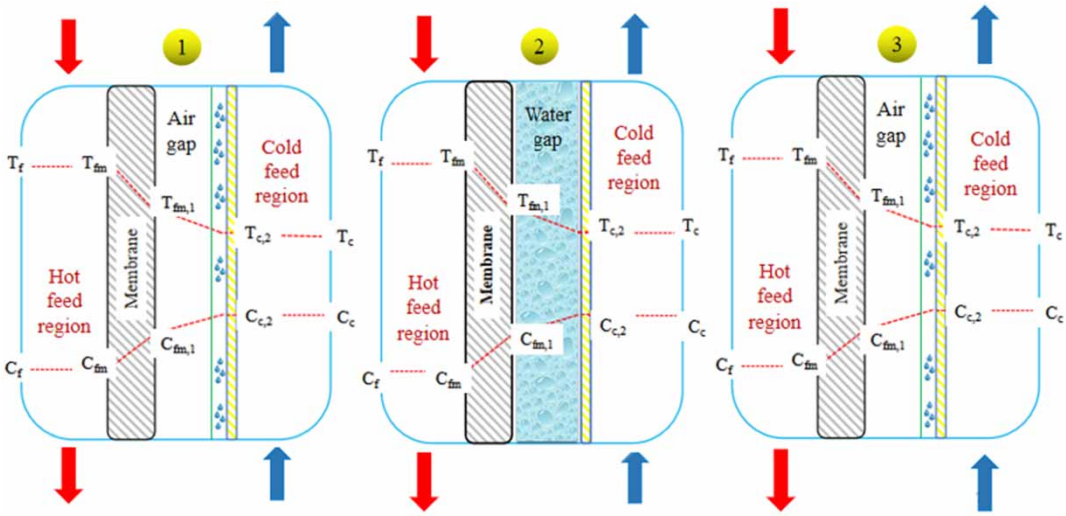

Figure 4 | The sketch elucidates no thermal-concentration boundary layers at the feed side of the three-stage air-gap–water-gap (AG-WG)MD system with high trans-membrane temperature difference.

Instrument Limited Company, China), and coolant DLSB-10 (Tianjin Xingke Instrument Limited Company, China).

Membrane and membrane module materials

The membrane modules prepared by our research team are manufactured from plexiglas and enclosed externally by thermal insulation to minimize the evaporation losses to the environment. The modules are designed to use polyvinylidene difluoride (PVDF) hollow fiber membranes with total effective area of 1.08 m^2 (0.36 m^2 each membrane module) and thickness of 150 μm, average pore size of 0.20 μm, and average porosity of 85%. The channels for evaporating and condensing in each module have 120 PVDF hollow fibers (0.18 m^2 interior membrane surface area) and 240 polypropylene (PP) acts as a heat exchange tube (0.18 m^2 interior membrane surface area). Inner/outer diameter ($m \times 10^{-3}$) of hollow fiber membranes (i.e., evaporating channels) and heat exchange tubes (i.e., condensing channels) are about 0.80/1.10 and 0.40/0.50 respectively. The total and effective length of hollow fiber membrane and heat exchange tube are around 0.77 m and 0.59 m, respectively. The gap width employed in the air-gap and water-gap modules is ≈5 mm.

Three-stage AGMD experiments

As illustrated in Figure 5(a), the feed solution was pumped from the feeding tank to the evaporator inlet channels in stages 1, 2, and 3, respectively by a circulation pump in the orientation from up to down. After the hot feed solution leaving the evaporator inlet channel in stage 3 flows into the coolant for temperature decrease, it then enters the condenser inlet channel in stages 3, 2, and 1, respectively as cold feed in a counter-current flow and then goes back to the feeding tank for a new circulation. To keep the feed volume and salt concentration constant inside the feeding tank throughout the experiment, the collected pure distilled water is returned to the feeding tank.

The performance of the systems was examined at different hot feed temperatures of 45 °C, 55 °C, 65 °C, and 75 °C, feed salt concentrations of 340 ppm, 7,500 ppm, 15,000 ppm, and 225,000 ppm, and feed flow rates of 15 l/h, 20 l/h, 25 l/h, and 30 l/h (flow velocities of 0.069 m/s, 0.092 m/s, 0.115 m/s, and 0.138 m/s and Reynolds numbers of 55.09, 73.45, 91.82, and 110.18, respectively). The temperature at the cold permeate side was kept stable at 20 °C. To make the obtained data more accurate and credible, each experiment was implemented three times under the same operating conditions for one hour operation time and average values are given. Prior to initiating the experiment, the laboratory-scale of various three-stage MD systems is left running for one hour to guarantee no dissolved gases in the feed stream, the gap area filled completely with permeate water, and reaching a steady-state.

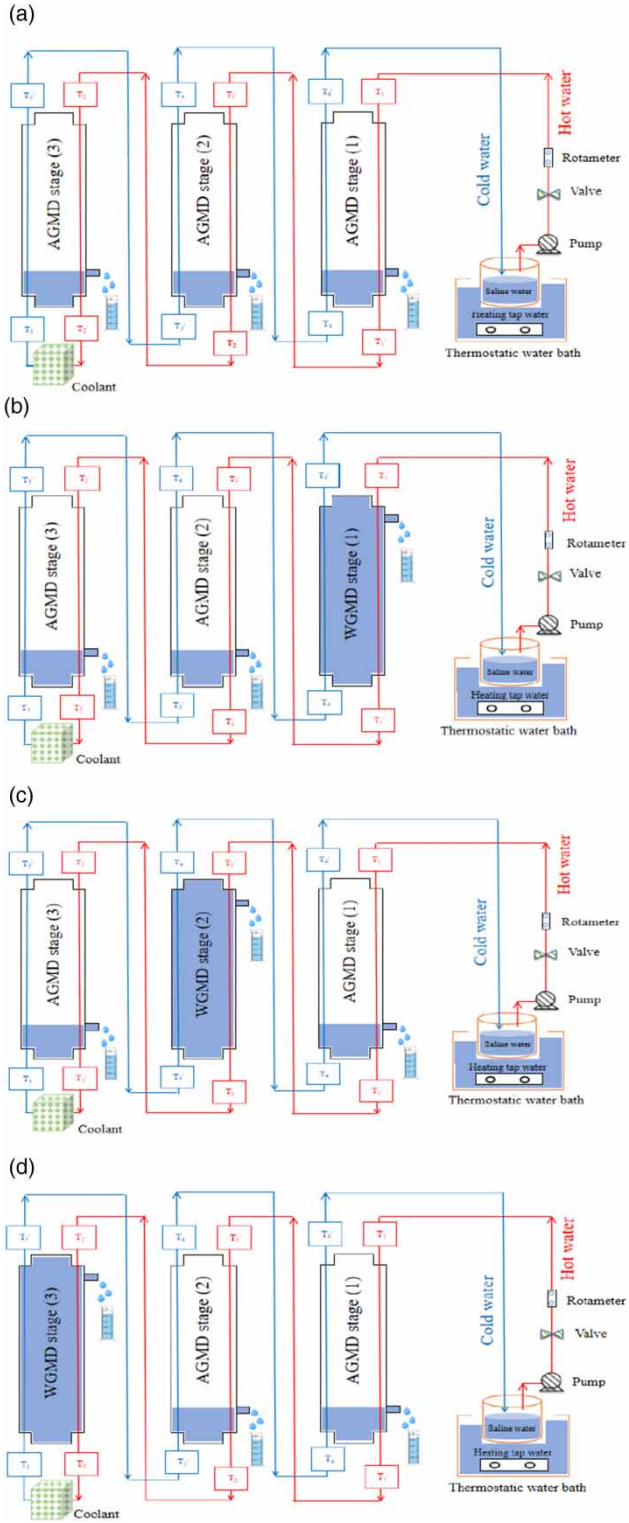

Figure 5 | The sketches show the different three-stage AGMD and (AG-WG)MD systems installed in a vertical direction: (a) (AG-AG-AG)MD reference system, (b) (WG-AG-AG)MD system, (c) (AG-WG-AG)MD system, (d) (AG-AG-WG)MD system.

In view of the difficulty of measuring the interface temperature at the membrane surface, the temperatures through and between each membrane module were continuously watched by several temperature sensors fixed at the inlets and outlets of the evaporator and the condenser channels and mean temperature differences are reported. The temperature controller XMTD-3001 (Easey Commercial Building, Hennessy Road, Wanchai, Hongkong, China) was used to control the hot inlet feed temperature. The vapor pressures of $P_{v,feed}$ and $P_{v,air\ gap}$ at feed and air-gap sides were viewed continuously using a manometer.

The obtained pure distilled water was weighed by electronic balance every ten minutes to note the variation of vapor flux. The electrical conductivity of the distilled water and saline feed were checked throughout using conductivity meter DDS-11A (Shanghai Leici Xinjing Instrument Company, China) to ensure the safety of the PVDF hollow fiber membrane and the quality of the pure distilled water.

Performance evaluation factors

The change in the system performance was evaluated by estimation of *GOR*, F_{wv}, *SRF*, $Q_{h.i}$, and *STEC*. The values of specific heat (C_{Pw}) and water density (ρ_w) utilized in the determination were obtained at ambient air temperature of 25 °C and are listed in Table 1. The experimental vapor flux (F_{wv}) with data errors are calculated and given in Tables 2–4.

The thermal energy consumed for yielding one kilogram of vapor flux (F_{wv}) can be obtained by:

$$STEC = \left[\frac{M_f \times C_{Pw} \times \rho_{sw}}{F_{wv} \times 36 \times 10^5}\right] \times \Delta T_{top},$$
$$\Delta T_{cross} = T_{evap.,\ inlet} - T_{cond.,\ outlet} \quad (16)$$

where *STEC* is the specific thermal energy consumption (kWh/kg), M_f is the feed flow rate (l/h), C_{Pw} is the specific heat of the feed (J/kg·°C), and ΔT_{cross} is the temperature difference between the evaporator inlet ($T_{evap.,inlet}$) and the condenser outlet ($T_{cond.,outlet}$) (°C).

The vapor flux (F_{wv}) in (kg/(m^2·h)) is given by:

$$F_{wv} = \left[\frac{W_{wv}}{ESA \times t}\right] \quad (17)$$

Table 1 | The various values of water density (ρ) and specific heat (C_{Pw}) obtained at different feed salt concentrations (C_f)

C_f (ppm)	C_{Pw} (kJ/kg·°C)	ρ_w (kg/m^3)
340	4.1865	996.95
7,500	4.1558	1,002.53
15,000	4.1387	1,008.22
22,500	4.1221	1,013.95

Table 2 | The experimental vapor flux (F_{wv}) at different feed temperatures (T_f)

T_f (°C)	(AG-AG-AG)MD	(WG-AG-AG)MD	(AG-WG-AG)MD	(AG-AG-WG)MD
kg/(m^2.h)				
45	2.12 ± 0.17	2.30 ± 0.21	2.50 ± 0.12	2.83 ± 0.27
55	2.36 ± 0.15	2.60 ± 0.17	2.79 ± 0.12	3.00 ± 0.21
65	2.53 ± 0.11	2.88 ± 0.30	3.00 ± 0.19	3.15 ± 0.15
75	2.88 ± 0.10	3.10 ± 0.11	3.27 ± 0.14	3.38 ± 0.19

Table 3 | The experimental vapor flux (F_{wv}) at different feed flow rates (M_f)

M_f (l/h)	(AG-AG-AG) MD	(WG-AG-AG) MD	(AG-WG-AG) MD	(AG-AG-WG) MD
kg/(m^2.h)				
15	2.17 ± 0.13	2.29 ± 0.11	2.66 ± 0.11	2.82 ± 0.16
20	2.36 ± 0.15	2.60 ± 0.17	2.79 ± 0.12	3.00 ± 0.21
25	2.66 ± 0.33	2.89 ± 0.10	3.00 ± 0.15	3.27 ± 0.13
30	2.97 ± 0.29	3.20 ± 0.11	3.27 ± 0.09	3.50 ± 0.13

Table 4 | The experimental vapor flux (F_{wv}) at different feed salt concentrations (C_f)

C_f (ppm)	(AG-AG-AG) MD	(WG-AG-AG) MD	(AG-WG-AG) MD	(AG-AG-WG) MD
kg/(m^2.h)				
340	2.66 ± 0.33	2.89 ± 0.10	3.66 ± 0.15	3.27 ± 0.13
7,500	2.50 ± 0.17	2.59 ± 0.08	2.77 ± 0.12	3.00 ± 0.21
15,000	2.31 ± 0.27	2.41 ± 0.18	2.60 ± 0.15	2.82 ± 0.16
22,500	2.10 ± 0.24	2.29 ± 0.25	2.24 ± 0.07	2.59 ± 0.10

where W_{wv} is the weight of distilled water during operation time t (kg), and ESA is the effective evaporation surface area in accordance with the interior membrane diameter (m^2).

The gained output ratio (GOR) can be described as (Çengel 2003):

$$GOR = \left[\frac{Q_{\text{l.h., distilled water}}}{Q_{\text{h.i}}}\right] \quad (18)$$

where $Q_{\text{l.h., distilled water}}$ and $Q_{\text{h.i}}$ refer to the latent heat of vaporization (≈2,326 kJ/kg) and specific waste heat input (MJ/kg). They are given by the following expressions:

$$Q_{\text{l.h., distilled water}} = F_{wv} \times \Delta H_V \quad (19)$$

$$Q_{\text{h.i.}} = M_f \times C_{Pw} \times \Delta T_{top} \quad (20)$$

Salt rejection factor (SRF) can be obtained as:

$$SRF = \left[\frac{C_{\text{saline water}} - C_{\text{distilled water}}}{C_{\text{saline water}}}\right] \times 100 \quad (21)$$

where $C_{\text{saline water}}$ and $C_{\text{distilled water}}$ are the salt concentrations of feed saline water and distilled water (%).

RESULTS AND DISCUSSION

Influences of feed temperature on the multi-stage (AG-WG)MD and one-stage AGMD system performances

The effect of feed temperature on vapor flux (F_{wv}) for the three-stage (AG-WG)MD and three-stage AGMD systems is elaborated in Figure 6(a). Feed temperature was changed between 45 °C and 75 °C at 5 °C intervals while flow rate, cooling water temperature, and feed salt concentration were kept at 20 l/h, 20 °C, and 340 ppm, respectively. Exponential flux increase with temperature that occurred in different multi-stage systems is attributed to the corresponding exponential vapor pressure increase. As shown in Figure 6(a), vapor flux for different systems of three-stage (AG-WG)MD was larger than that in the three-stage AGMD system. The flux was raised by 8.49%, 10.17%, 13.83%, 7.64%; 17.92%, 18.22%, 18.58%, 13.54%; and 33.49%, 27.12%, 24.51%, 17.36% at 45 °C, 55 °C, 65 °C, and 75 °C respectively. The improved flux is ascribed to the low effective air-gap and high driving force thanks to the incorporated water-gap while in the system of three-

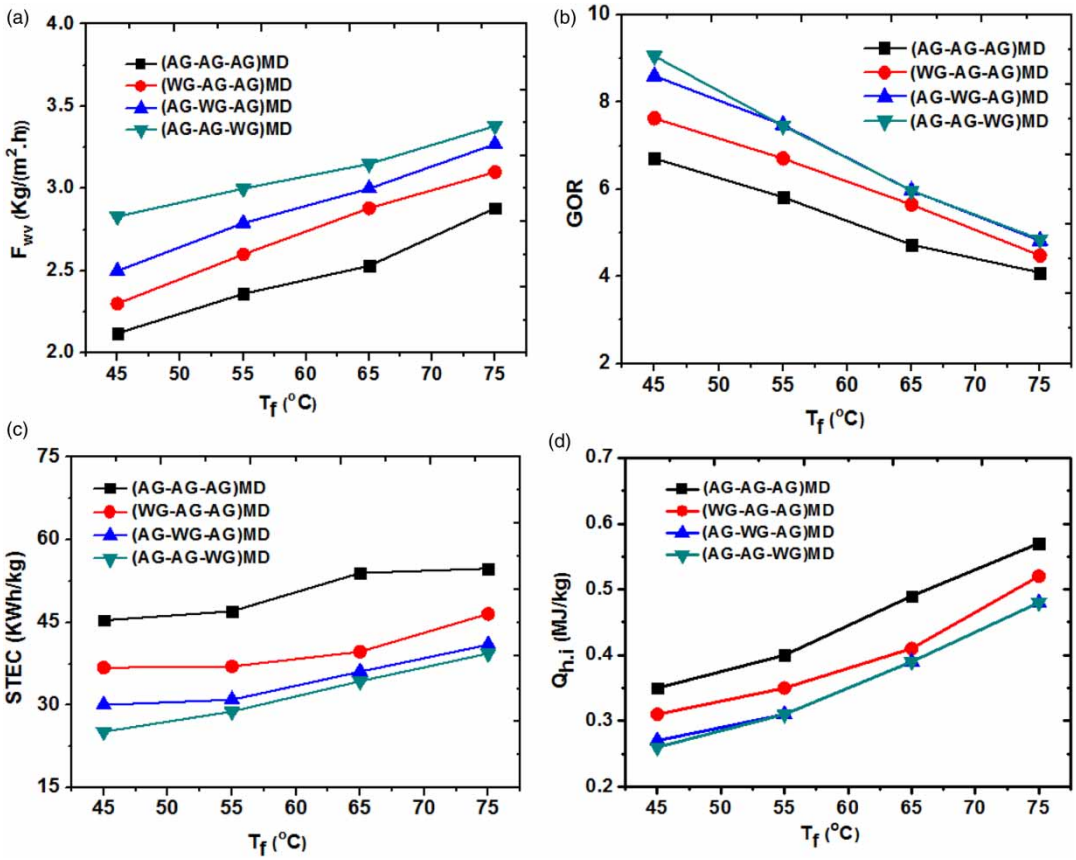

Figure 6 | Effect of different feed temperatures on the (a) F_{wv}, (b) GOR, (c) STEC, and (d) $Q_{h,i}$ for the three-stage (AG-WG)MD and AGMD systems.

stage AGMD the air-gap impeded vapor mass transfer and the temperature decrease per stage leading to flux reduction.

In comparison with other systems like two-stage (AG-WG) MD and one-stage AGMD, the three-stage (AG-WG)MD systems enhanced the flux around 17.59%, 12.90%, 12.31%, 13.64%, and 211.69%, 204.35%, 138.89%, 118.12% at 45 °C, 55 °C, 65 °C, and 75 °C, respectively. Similarly, the three-stage AGMD system gave extreme improvement in flux of about 32.50%, 6.79%, 8.12%, 17.55%, and 175.32%, 156.52%, 100.79%, 93.29% compared with other two-stage AGMD and one-stage AGMD systems. As for salt rejection factor (SRF), different quantities of pure distilled water were produced from different systems, and the employed PVDF porous membrane demonstrated high SRF reaching up to 99.7%.

As presented in Figure 6(b), various systems of three-stage (AG-WG)MD attained higher GOR than that of the three-stage AGMD system, reaching up to 13.71%, 15.29%, 19.45%, 9.54%; 28.17%, 28.52%, 26.22%, 17.85%; and 35.02%, 28.18%, 26.22%, 18.58%. The high GOR related to conductive heat loss reduction and trans-membrane temperature difference (ΔT_{cross}) increased by 4.54%, 4.42%, 4.70%, 1.53%; 7.95%, 7.96%, 6.04%, 3.57%; and 1.14%, 0.88%, 1.34%, 1.02%. On the other side, the low GOR in the case of the three-stage AGMD system was attributed to the small amount of thermal energy utilized to produce vapor relative to the energy used for warming the inlet feed stream. Additionally, poor cooling of the air gap compared with the water gap was because of the lower specific heat capacity of air by 4.23 times than that of water (i.e., C_{Pw} of air = 993 J/(kg·°C) and C_{Pw} of water = 4,200 J/(kg·°C)).

In comparison with the two-stage (AG-WG)MD and one-stage AGMD systems, GOR for the three-stage (AG-WG)MD systems was increased profoundly by 60.57%, 42.69%, 19.11%, 2.16%, and 204.33%, 172.45%, 162.78%, 136%. In like manner, the system of three-stage AGMD enhanced GOR about 31.83%, 17.81%, 2.60%,

3.54%, and 142.24%, 119.62%, 112.11%, 104.50% compared with two-stage AGMD and one-stage AGMD systems. The percentage increases in GOR for the three-stage (AG-WG)MD systems were greater compared with the three-stage AGMD system except at a temperature of 75 °C for two-stage (AG-WG)MD and two-stage AGMD systems.

The main cause behind GOR enhancement in the case of the three-stage (AG-WG)MD systems was an efficient internal heat recycling introduced by the integrated water-gap module, leading to thermal energy reduction. Vapor flux and thermal power consumption over experimental time were utilized to realize the STEC using Equation (16). As can be noticed from Figure 6(c), the various systems of three-stage (AG-WG)MD consumed less thermal energy compared with the three-stage AGMD system. The STEC values read for the (WG-AG-AG)MD, (AG-WG-AG)MD, and (AG-AG-WG)MD systems were 36.81–46.55 kWh/kg, 30.04–40.97 kWh/kg, and 25.18–39.36 kWh/kg, respectively while the corresponding value in the (AG-AG-AG)MD system was 45.39–54.77 kWh/kg. Identically, the $Q_{h.i}$ values were 0.31–0.52 MJ/kg, 0.27–0.48 MJ/kg, and 0.26–0.48 MJ/kg, and the corresponding value in the case of (AG-AG-AG)MD was 0.35–0.57 MJ/kg (Figure 6(d)).

Influences of feed flow rate on the multi-stage (AG-WG)MD and one-stage AGMD system performances

Figure 7(a) demonstrates the quantity of vapor flux resulted from the systems of three-stage (AG-WG)MD and three-stage AGMD as a function of feed flow rate at constant feed temperature of 55 °C, cooling water temperature of 20 °C, and feed salt concentration of 340 ppm. As can be noticed from Figure 7(a), the flux quantity of the various three-stage (AG-WG)MD systems was maximal compared with the three-stage AGMD system. Compared with the system of (AG-AG-AG)MD, the systems of (WG-AG-AG)MD, (AG-WG-AG)MD, and (AG-AG-WG)MD boosted vapor flux by about 5.53%, 10.17%, 8.65%, 7.74%; 22.58%, 18.22%, 12.78%, 10.10%; and 29.95%, 27.12%, 22.93%, 17.85% at 15 l/h, 20 l/h, 25 l/h, and 30 l/h, respectively. The possible reasons for high flux were assigned to an obvious temperature-concentration polarization reduction and low impedance to vapor molecules condensing instantly at the membrane/water-gap interface.

The three-stage (AG-WG)MD systems developed flux by 38.50%, 12.90%, 2.69%, 1.53%, and 223.75%, 204.35%, 127.61%, 124.32% compared with the other two-stage (AG-WG)MD and one-stage AGMD systems, respectively. Also, the three-stage AGMD systems enhanced flux remarkably by 82.35%, 6.79%, 4.72%, 4.58%, and 171.25%, 156.52%, 98.51%, 100.78% compared with the other two-stage AGMD and one-stage AGMD, respectively. The fabricated hydrophobic PVDF hollow fiber membrane used in the experiment rejected around 99.7% of salts at different feed flow rates.

Figure 7(b) advertises that the various three-stage (AG-WG)MD systems performed with better GOR than the three-stage AGMD system, reaching up to 7.79%, 15.29%, 15.17%, 18.02%; 27.90%, 28.52%, 22.52%, 26.66%; and 30.98%, 28.18%, 25.83%, 21.40%. The enhancement of GOR was associated with the following factors: firstly, changing the mass and heat transfer significantly by virtue of permeated water filling the gap; secondly, increasing the amount of heat absorbed through the cold feed stream and decreasing the conductive heat loss across the membrane; thirdly, raising the ΔT_{cross} by 2.05%, 4.42%, 5.62%, 8.70%; 4.11%, 7.96%, 7.87%, 13.04%; and 0.68%, 0.88%, 2.25%, 2.90%.

The three-stage (AG-WG)MD systems increased GOR by about 35.27%, 42.69%, 33.17%, 37.91%, and 197.36%, 172.45%, 175.43%, 204.69% compared with the other two-stage (AG-WG)MD and one-stage AGMD systems. Also, the GOR of the three-stage AGMD systems was enhanced appreciably by 34.96%, 17.81%, 27.83%, 34.29%, and 143.17%, 119.62%, 127.30%, 149.69% compared with the other two-stage AGMD and one-stage AGMD systems, respectively. This result could be explained by the effective role of the water-gap module in reducing the thermal-concentration boundary layer thickness at the membrane surface. Consequently, increasing the GOR economized the energy required for heating and decreased extremely the waste heat input into the system as illustrated in Figure 7(c) and 7(d).

As seen from Figure 7(c), the absence of the water-gap module negatively affected the heat recovery in the (AG-AG-AG)MD system, leading to high STEC. High recorded STEC were between 27.20 and 53.90 kWh/kg corresponding to low STEC in the (WG-AG-AG)MD, (AG-WG-AG)MD, and (AG-AG-WG)MD systems around

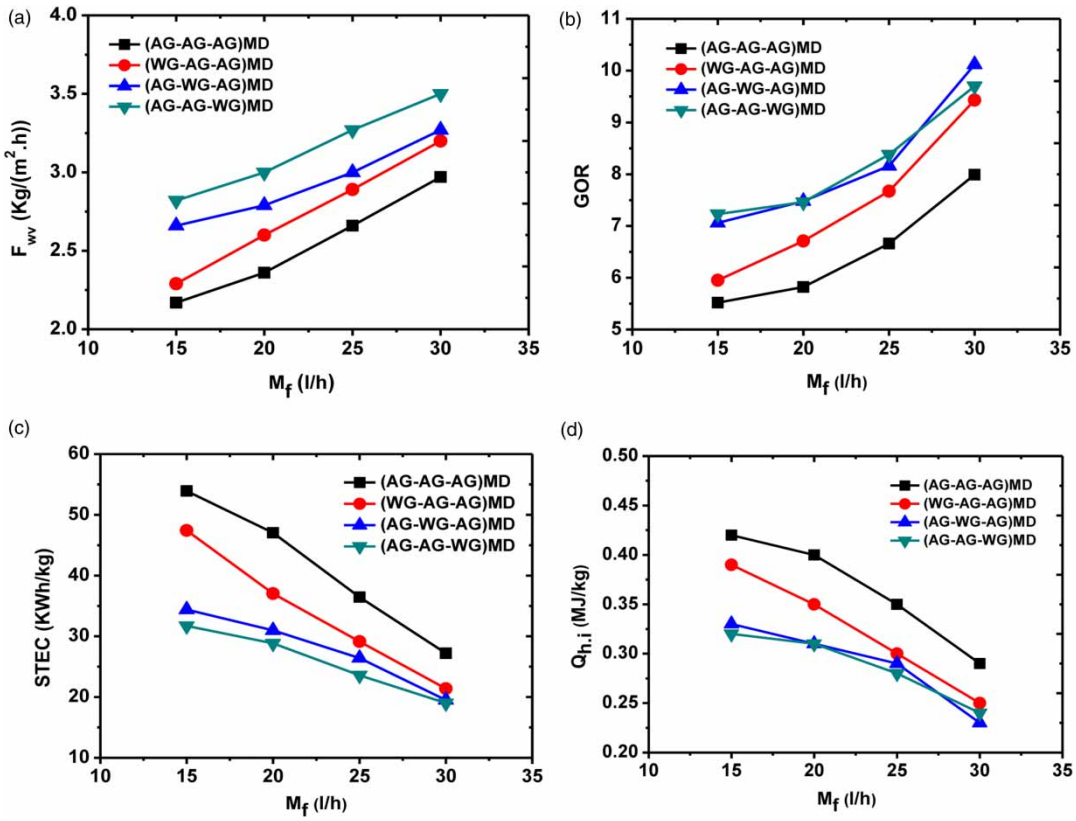

Figure 7 | Effect of different feed flow rates on the (a) F_{wv}, (b) GOR, (c) STEC, and (d) $Q_{h.i}$ for the three-stage (AG-WG)MD and AGMD systems.

21.39–47.41 kWh/kg, 19.51–34.40 kWh/kg, and 19.02–31.70 kWh/kg, respectively. Likewise, the $Q_{h.i}$ in the (AG-AG-AG)MD system were in the range of 0.29–0.42 MJ/kg corresponding to 0.25–0.39 MJ/kg, 0.23–0.33 MJ/kg, and 0.24–0.32 MJ/kg (Figure 7(d)).

Influences of feed salt concentration on the multi-stage (AG-WG)MD and one-stage AGMD system performances

The variation of flux with feed salt concentration for the systems of three-stage (AG-WG)MD and three-stage AGMD is characterized in Figure 8(a). Experiments were conducted at a constant temperature of 55 °C, cooling water temperature of 20 °C, and feed flow rate of 25 l/h. A remarkable flux decline with salt concentration was due to parallel vapor pressure decrease at the feed side for the investigated systems. As can be perceived from Figure 8(a), the maximal flux of the three-stage (AG-WG)MD systems was imputed to low concentration polarization influence by virtue of the incorporated water-gap module. The (WG-AG-AG)MD, (AG-WG-AG)MD, and (AG-AG-WG)MD systems improved flux by 8.65%, 3.60%, 4.33%, 9.05%; 12.78%, 10.80%, 12.55%, 15.24%; and 22.93%, 20%, 22.08%, 23.33% compared with the (AG-AG-AG)MD system at 340 ppm, 7,500 ppm, 15,000 ppm, and 22,500 ppm, respectively.

Respecting the flux comparison, three-stage (AG-WG)MD boosted the system flux by 2.69%, 3.72%, 5.24%, 10.96% and 127.61%, 138.46%, 161%, 179.31% compared with the other systems of two-stage (AG-WG)MD and one-stage AGMD. Also, the three-stage AGMD system upgraded the flux by 4.72%, 9.65%, 10%, 9.95% and 98.51%, 113.68%, 131%, 141.38% as compared with the other two-stage AGMD and one-stage AGMD. For the salt rejection factor (SRF), increased feed salt concentration from 340 ppm to 22,500 ppm resulting in a tenuous decrease in the separation efficiency of the PVDF hollow fiber membrane ranging from 99.7% to 99.5%.

As shown in Figure 8(b), increases of 15.17%, 8.39%, 10.84%, 13.67%; 22.52%, 17.27%, 21.88%, 24.13%; and

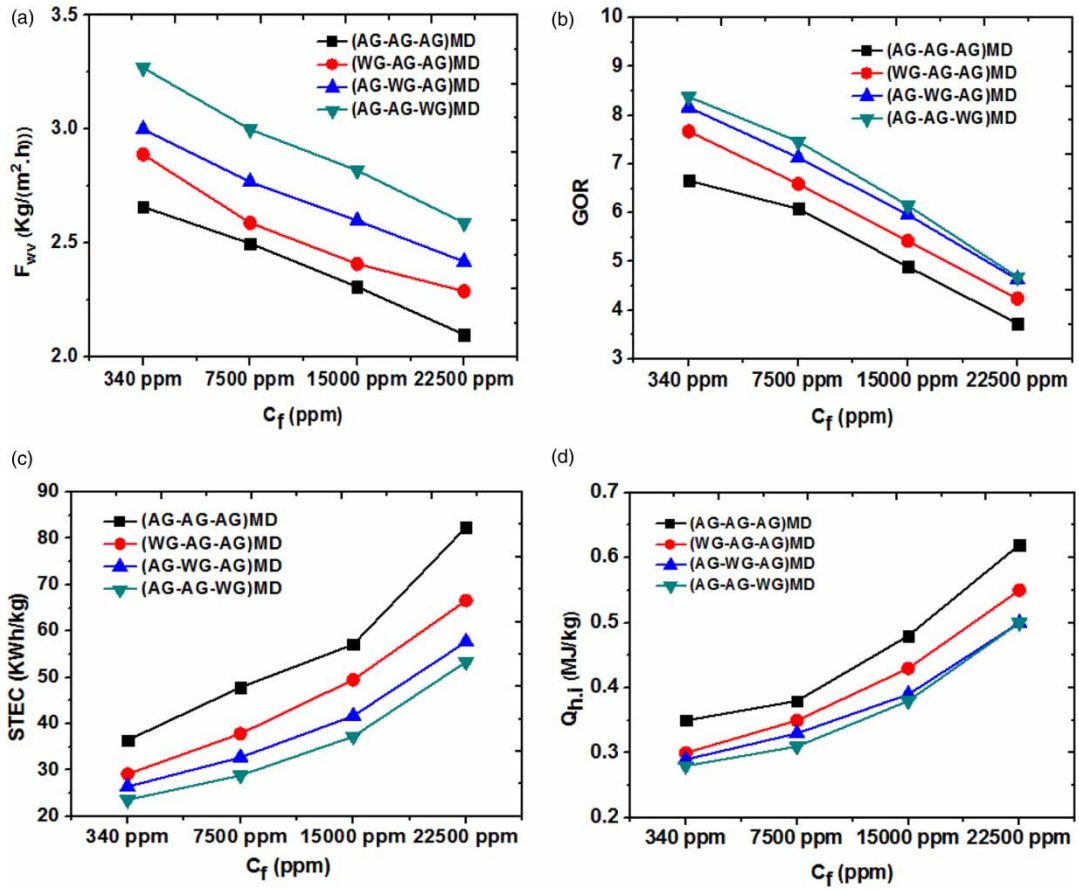

Figure 8 | Effect of different feed salt concentrations on the (a) F_{wv}, (b) GOR, (c) STEC, and (d) $Q_{h,i}$ for the three-stage (AG-WG)MD and AGMD systems.

25.83%, 22.70%, 25.77%, 25.47% were accomplished in GOR for the (WG-AG-AG)MD, (AG-WG-AG)MD, (AG-AG-WG)MD systems compared with the (AG-AG-AG)MD system. This result enhanced ΔT_{cross} by 5.62%, 4.35%, 5.66%, 3.94%; 7.87%, 5.43%, 7.55%, 7.09%; and 2.25%, 2.17%, 2.83%, 1.57%. In comparison with the two-stage (AG-WG)MD and one-stage AGMD systems, the three-stage (AG-WG)MD systems increased GOR by 33.17%, 35.25%, 21.16%, 2.96% and 175.43%, 168.44%, 171.63%, 255.91%, respectively. Similarly, the three-stage AGMD system promoted GOR about 27.83%, 24.59%, 8.67%, 3.90% and 127.30%, 131.18%, 127.44%, 193.70% compared with the two-stage AGMD and one-stage AGMD.

In connection with the STEC in the case of the three-stage AGMD system higher values were registered compared with the three-stage (AG-WG)MD. The (AG-AG-AG)MD system recorded STEC between 36.82 and 82.43 kWh/kg corresponding to 29.14–66.59 kWh/kg, 26.40–57.68 kWh/kg, and 23.57–53.34 kWh/kg in (WG-AG-AG)MD, (AG-WG-AG)MD, and (AG-AG-WG)MD, respectively (Figure 8(c)). Likewise, the $Q_{h,i}$ of the (AG-AG-AG)MD system was between 0.35 and 0.62 MJ/kg corresponding to 0.30–0.55 MJ/kg, 0.29–0.50 MJ/kg, and 0.28–0.50 MJ/kg in (WG-AG-AG), (AG-WG-AG), and (AG-AG-WG)MD (Figure 8(d)).

Under all the above-mentioned studied operating conditions (feed temperature, flow rate, and salt concentration), the GOR values obtained for the conventional multi-stage AGMD system which operated without a water-gap module are low, while the GOR values for the novel three-stage (AG-AG-WG)MD system operated with a water-gap module are high. As well, the STEC considered in this experiment refers to the heat that is continuously replenished by the heater during the circulation. Due to efficient internal heat recovery unlike the conventional MD systems, the circulating cold feed will absorb a part of the heat from the steam condensation, which results in a

reduction in the heat (energy consumption) provided by the external heater during the cycle, thereby achieving a high GOR and vapor flux for the novel three-stage (AG-AG-WG)MD system.

Flux comparison with the published literature

Table 5 shows a vapor flux comparison between the novel three-stage (AG-AG-WG)MD system investigated in this study and other conventional multi-stage AGMD systems reported in the the published literature. In this study, the novel (AG-AG-WG)MD system was assessed by comparing it with conventional (AG-AG-AG)MD systems. It was found that the system of (AG-AG-WG)MD performed better compared with (AG-AG-AG)MD using the same PVDF hollow fiber membrane under the same operating parameters. However, variations in flux were observed when our novel (AG-AG-WG)MD system was compared with other experimental works because of a variance in different operating conditions and membrane characteristics as well. As listed in Table 5, these variations result from decreasing the air gap width (δ_{gap} = 4 mm) and increasing the pore size (0.45 μm) (Khalifa & Alawad 2018). Additionally, increase of feed temperature and flow rate, decrease of membrane thickness, coolant temperature, and feed salt concentration promoted the flux as revealed by some authors (e.g. Bahar *et al.* 2014; Geng *et al.* 2015). In conclusion, different operating conditions and membrane characteristics induced various fluxes as seen in Table 5. Therefore, if all multi-stage MD systems examined used the same membrane under the same operating parameters, our novel system will be outperformed.

CONCLUSIONS

In this research work, the water-gap module improved profoundly the performance of the three-stage air-gap membrane distillation (AGMD) system. The new three-stage air-gap–water-gap membrane distillation (AG-WG)MD system reduced deeply the energy consumption and increased the vapor flux due to efficient internal heat recycling introduced by the water-gap module. At optimal operating conditions involving a hot feed temperature of 45 °C, feed flow rate of 20 l/h, cooling water temperature of 20 °C, and feed salt concentration of 340 ppm, the system of three-stage (AG-WG)MD promoted the flux by 17.59% and 211.69%, and gained output ratio (GOR) by 60.57% and 204.33% compared with other systems of two-stage (AG-WG)MD and one-stage AGMD, respectively. The salt rejection factor (SRF) registered was on average about 99.5% at highest salt concentration. In the present research work emerged experimentally the effective role of the water-gap module in reducing the

Table 5 | Comparisons between the flux (F_{wv}) of the novel three-stage (AG-AG-WG)MD system in the present study and different values reported in the published literature

	Hydrophobic micro-porous membrane			Multi-stage AGMD system	F_{wv} (kg/(m^2.h))
Reference	Kind	Characteristics	Operating parameters		
Present study	PVDF Hollow fiber	Thickness = 150 μm, porosity = 85%, pore size = 0.20 μm, contact angle = 80.5°, bubble point pressure = 0.11 MPa	T_f = 55 °C, T_c = 20 °C, M_f = 30 l/h, δ_{gap} = 5 mm, C_f = 340 ppm (tap water)	(AG-AG-WG)MD	3.50
Khalifa & Alawad (2018)	PTFE Flat plate	Porosity = 80%, pore size = 0.45 μm, contact angle = 140°	T_f = 50 °C, T_c = 20 °C, M_f = 2.3 l/min, δ_{gap} = 4 mm, C_f = 150 mg/L (tap water)	Three-stage AGMD	Ranging from 4.0 to 6.0
Bahar *et al.* (2014)	PVDF Flat sheet	Thickness = 125 μm, porosity = 75%, pore size = 0.45 μm, bubble point pressure ≥ 0.75 MPa, effective membrane area = 88.2 cm^2	T_f = 50 °C, T_c = 10 °C, M_f = 35 ml/min, δ_{gap} = 2.5 mm, C_f = 176 ppm (tap water)	Three-stage AGMD	Ranging from 11.0 to 12.0
Geng *et al.* (2015)	PP Hollow fiber	Porosity = 71%, pore size = 0.23 μm, effective internal membrane area = 0.95 m^2	T_f = 95 °C, T_c = 45 °C, M_f = 80 l/h, δ_{gap} = 0.5 mm, C_f = 62.5 g/L (artificial RO brine)	Four-stage AGMD	4.20

boundary layer thickness and improve the flux. Consequently, increasing the flux and GOR economized mightily the energy required for heating and decreased waste heat input into the system. Also, the number of stages could be increased with high flux and more operation stability.

ACKNOWLEDGEMENTS

Supported by the Program for Innovative Research Team in University of Tianjin (No. TD13-5044). Supported by the Program for Changjiang Scholars and Innovative Research Team in University (PCSIRT) of Ministry of Education of China (Grand no. IRT17_R80). National Center for International Joint Research on Separation Membranes, Tianjin Polytechnic University, Tianjin 300387, China.

DATA AVAILABILITY STATEMENT

All relevant data are included in the paper or its Supplementary Information.

REFERENCES

Abu-Zeid, M. A. E.-R. & ElMasry, G. 2020 Experimental evaluation of two consecutive air-gap membrane distillation modules with heat recovery. *Water Supply* **20** (5), 1678–1691.

Alkhudhiri, A., Darwish, N. & Hilal, N. 2012 Membrane distillation: a comprehensive review. *Desalination* **287**, 2–18.

Alsaadi, A. S., Ghaffour, N., Li, J.-D., Gray, S., Francis, L., Maab, H. & Amy, G. L. 2013 Modeling of air-gap membrane distillation process: a theoretical and experimental study. *Journal of Membrane Science* **445**, 53–65.

Alsaadi, A. S., Francis, L., Maab, H., Amy, G. L. & Ghaffour, N. 2015 Evaluation of air gap membrane distillation process running under sub-atmospheric conditions: experimental and simulation studies. *Journal of Membrane Science* **489**, 73–80.

Bahar, R., Hawlader, M. N. A., Ng, K. C. & Haw, Y. J. 2014 Experimental study on a multi-stage air gap membrane distillation (AGMD) unit. *Jurnal Teknologi (Sciences & Engineering)* **69** (9), 89–92. doi:10.11113/jt.v69.3403.

Bouguecha, S., Chouikh, R. & Dhahbi, M. 2002 Numerical study of the coupled heat and mass transfer in membrane distillation. *Desalination* **152**, 245–252.

Cath, T. Y., Adams, V. D. & Childress, A. E. 2004 Experimental study of desalination using direct contact membrane distillation: a new approach to flux enhancement. *Journal of Membrane Science* **228**, 5–16.

Çengel, Y. A. 2003 *Heat Transfer: A Practical Approach*, 2nd edn. McGraw-Hill, Boston, MA, USA.

Cipollina, A., Di Sparti, M. G., Tamburini, A. & Micale, G. 2012 Development of a membrane distillation module for solar energy seawater desalination. *Chemical Engineering Research and Design* **90** (12), 2101–2121.

Cussler, E. L. 1997 *Diffusion: Mass Transfer in Fluid Systems*, 2nd edn. Cambridge University Press, Cambridge, UK.

Ding, Z., Liu, L., El-Bourawi, M. S. & Ma, R. 2005 Analysis of a solar-powered membrane distillation system. *Desalination* **172**, 27–40.

Duong, H. C., Chivas, A. R., Nelemans, B., Duke, M., Gray, S., Cath, T. Y. & Nghiem, L. D. 2015 Treatment of RO brine from CSG produced water by spiral-wound air gap membrane distillation – a pilot study. *Desalination* **366**, 121–129.

Ebadi, M., Mozdianfard, M. R. & Aliabadi, M. 2019 Employing full factorial design and response surface methodology for optimizing direct contact membrane distillation operational conditions in desalinating the rejected stream of a reverse osmosis unit at Esfahan refinery – Iran. *Water Supply* **19** (2), 492–501.

El-Bourawi, M. S., Ding, Z., Ma, R. & Khayet, M. 2006 A framework for better understanding membrane distillation separation process. *Journal of Membrane Science* **285**, 4–29.

Francis, L., Ghaffour, N., Alsaadi, A. A. & Amy, G. L. 2013 Material gap membrane distillation: a new design for water vapor flux enhancement. *Journal of Membrane Science* **448**, 240–247.

García-Payo, M. C., Izquierdo-Gil, M. A. & Fernández-Pineda, C. 2000 Air gap membrane distillation of aqueous alcohol solutions. *Journal of Membrane Science* **169** (1), 61–80.

Geng, H. X., He, Q. F., Wu, H. Y., Li, P. L., Zhang, C. Y. & Chang, H. Y. 2014 Experimental study of hollow fiber AGMD modules with energy recovery for high saline water desalination. *Desalination* **344**, 55–63.

Geng, H. X., Wang, J., Zhang, C. Y., Li, P. L. & Chang, H. Y. 2015 High water recovery of RO brine using multi-stage air gap membrane distillation. *Desalination* **355**, 178–185.

González-Bravo, R., Nápoles-Rivera, F., Ponce-Ortega, J. M., Nyapathi, M., Elsayed, N. & El-Halwagi, M. M. 2015 Synthesis of optimal thermal membrane distillation networks. *AIChE Journal* **61**, 448–463.

Guijt, C. M., Meindersma, G. W., Reith, T. & de Haan, A. B. 2005 Air gap membrane distillation: 2. Model validation and hollow fibre module performance analysis. *Separation and Purification Technology* **43**, 245–255.

Guillén-Burrieza, E., Blanco, J., Zaragoza, G., Alarcón, D.-C., Palenzuela, P., Ibarra, M. & Gernjak, W. 2011 Experimental analysis of an air gap membrane distillation solar desalination pilot system. *Journal of Membrane Science* **379**, 386–396.

Guo, H. F., Ali, H. M. & Hassanzadeh, A. 2016 Simulation study of flat-sheet air gap membrane distillation modules coupled with an evaporative crystallizer for zero liquid discharge water desalination. *Applied Thermal Engineering* **108**, 486–501.

Hawlader, M. N. A., Bahar, R., Ng, K. C. & Stanley, L. J. W. 2012 Transport analysis of an air gap membrane distillation (AGMD) process. *Desalination and Water Treatment* **42**, 333–346.

Hickenbottom, K. L. & Cath, T. Y. 2014 Sustainable operation of membrane distillation for enhancement of mineral recovery from hypersaline solutions. *Journal of Membrane Science* **454**, 426–435.

Hogan, P. A., Sudjito Fane, A. G. & Morrison, G. L. 1991 Desalination by solar heated membrane distillation. *Desalination* **81**, 81–90.

Khalifa, A. E. 2015 Water and air gap membrane distillation for water desalination – an experimental comparative study. *Separation and Purification Technology* **141**, 276–284.

Khalifa, A. E. & Alawad, S. M. 2018 Air gap and water gap multistage membrane distillation for water desalination. *Desalination* **437**, 175–183.

Khalifa, A. E., Lawal, D. U. & Antar, M. A. 2014 Performance of air gap membrane distillation unit for water desalination. In: *Proceedings of the ASME 2014 International Mechanical Engineering Congress and Exposition IMECE2014 November 14–20*, Montreal, Quebec, Canada.

Khalifa, A., Lawal, D., Antar, M. & Khayet, M. 2015 Experimental and theoretical investigation on water desalination using air gap membrane distillation. *Desalination* **376**, 94–108.

Khalifa, A. E., Alawad, S. M. & Antar, M. A. 2017 Parallel and series multistage air gap membrane distillation. *Desalination* **417**, 69–76.

Khayet, M. & Matsuura, T. 2011 *Membrane Distillation: Principles and Applications*. Elsevier, Amsterdam, The Netherlands.

Kim, Y.-D., Thu, K. & Choi, S.-H. 2015 Solar-assisted multi-stage vacuum membrane distillation system with heat recovery unit. *Desalination* **367**, 161–171.

Koschikowski, J., Wieghaus, M., Rommel, M., Ortin, V. S., Suarez, B. P. & Betancort Rodríguez, J. R. 2009 Experimental investigations on solar driven stand-alone membrane distillation systems for remote areas. *Desalination* **248**, 125–131.

Laganà, F., Barbieri, G. & Drioli, E. 2000 Direct contact membrane distillation: modelling and concentration experiments. *Journal of Membrane Science* **166**, 1–11.

Lawal, D. U. & Khalifa, A. E. 2015 Experimental investigation of an air gap membrane distillation unit with double-sided cooling channel. *Desalination and Water Treatment* **57**, 11066–11080.

Lee, J.-G. & Kim, W.-S. 2014 Numerical study on multi-stage vacuum membrane distillation with economic evaluation. *Desalination* **339**, 54–67.

Lee, J.-G., Kim, W.-S., Choi, J.-S., Ghaffour, N. & Kim, Y.-D. 2016 A novel multi-stage direct contact membrane distillation module: design, experimental and theoretical approaches. *Water Research* **107**, 47–56.

Lee, J.-G., Alsaadi, A. S. & Ghaffour, N. 2019 Multi-stage air gap membrane distillation reversal for hot impaired quality water treatment: concept and simulation study. *Desalination* **450**, 1–11.

Lu, K.-J., Zuo, J. & Chung, T.-S. 2017 Novel PVDF membranes comprising n-butylamine functionalized graphene oxide for direct contact membrane distillation. *Journal of Membrane Science* **539**, 34–42.

Martínez, L. & Rodríguez-Maroto, J. M. 2008 Membrane thickness reduction effects on direct contact membrane distillation performance. *Journal of Membrane Science* **312**, 143–156.

Minier-Matar, J., Hussain, A., Janson, A., Benyahia, F. & Adham, S. 2014 Field evaluation of membrane distillation technologies for desalination of highly saline brines. *Desalination* **351**, 101–108.

Pangarkar, B. L. & Deshmukh, S. K. 2015 Theoretical and experimental analysis of multi-effect air gap membrane distillation process (ME-AGMD). *Journal of Environmental Chemical Engineering* **3** (3), 2127–2135.

Saffarini, R. B., Summers, E. K., Arafat, H. A. & Lienhard V, J. H. 2012 Technical evaluation of stand-alone solar powered membrane distillation systems. *Desalination* **286**, 332–341.

Schwantes, R., Cipollina, A., Gross, F., Koschikowski, J., Pfeifle, D., Rolletschek, M. & Subiela, V. 2013 Membrane distillation: solar and waste heat driven demonstration plants for desalination. *Desalination* **323**, 93–106.

Shahu, V. T. & Thombre, S. B. 2020 Analysis and optimization of a new cylindrical air gap membrane distillation system. *Water Supply* **20** (1), 361–371.

Sharqawy, M. H., Lienhard V, J. H. & Zubair, S. M. 2010 Thermophysical properties of seawater: a review of existing correlations and data. *Desalination and Water Treatment* **16** (1–3), 354–380.

Shim, S. M., Lee, J. G. & Kim, W. S. 2014 Performance simulation of a multi-VMD desalination process including the recycle flow. *Desalination* **338**, 39–48.

Sivakumar, M., Ramezanianpour, M. & O'Halloran, G. 2015 Brackish water treatment for reuse using vacuum membrane distillation process. *Water Supply* **15** (2), 362–369.

Wang, P. & Chung, T.-S. 2015 Recent advances in membrane distillation processes: membrane development, configuration design and application exploring. *Journal of Membrane Science* **474**, 39–56.

Xu, J., Singh, Y. B., Amy, G. L. & Ghaffour, N. 2016 Effect of operating parameters and membrane characteristics on air gap membrane distillation performance for the treatment of highly saline water. *Journal of Membrane Science* **512**, 73–82.

Yao, K., Qin, Y. J., Yuan, Y. J., Liu, L. Q., He, F. & Wu, Y. 2012 A continuous-effect membrane distillation process based on hollow fiber AGMD module with internal latent-heat recovery. *AIChE Journal* **59** (4), 1278–1297.

Zhang, J., Duke, M., Ostarcevic, E., Dow, N., Gray, S. & Li, J.-d. 2009 Performance of new generation membrane distillation membranes. *Water Supply* **9** (5), 501–508.

Zhao, K., Heinzl, W., Wenzel, M., Büttner, S., Bollen, F., Lange, G., Heinzl, S. & Sarda, N. 2013 Experimental study of the memsys vacuum-multi-effect-membrane-distillation (V-MEMD) module. *Desalination* **323**, 150–160.

First received 18 March 2020; accepted in revised form 29 July 2020. Available online 11 August 2020